CHAPTER III

Mitigation of Mutual Coupling in Linear Array Systems Incorporating Metasurface Superstrate

3.1. Introduction

3.2. Design of the metasurface

3.2.1. Decoupling mechanism

3.2.2. Design of the metasurface unit cell

3.3. Mutual coupling reduction in linear patch array

3.3.1. Unit antenna and 1×3 antenna array design

3.3.2. 1×3 antenna array-metasurface assembly

3.3.3. Parametric optimization of the 1×3 array-metasurface assembly

3.3.4. 1×7 antenna array-metasurface assembly

3.4. Implementation of the design

3.4.1. S_{11} and radiation pattern measurement technique

3.4.2. Fabrication and performance study of 1×3 antenna array and metasurface assembly

3.4.3. Fabrication and performance study of 1×3 antenna array and metasurface assembly

3.5. Chapter summary

Reference

3.1. INTRODUCTION

Mutual coupling in an antenna array refers to the electromagnetic interaction between the antenna elements in an array. In applications like tracking radars, satellite communication radars etc., high gain phased array antennas (PAAs) are needed, which requires large number of antennas [1]. Two types of coupling phenomena are commonly discussed in the literature [2]. The first is surface-wave coupling, which occurs within the substrate material and propagates along its surface. The second is space-wave coupling, associated with near-field or reactive-field interactions, and takes place in the region above the substrate, primarily between the closely spaced radiating antennas as shown in Figure 3.1(a). The near field space coupling is generally dominant in case of printed antennas on low permittivity substrates [3] and generally effects cross-polar radiation characteristic, scanning range and active return loss in an antenna arrays [4]. The coupling becomes more pronounced in a compact high gain array systems where the interelement spacing $< \lambda/2$. This puts paradoxical limitations to the extent of inter-elemental spacing [5] and performance of the array.

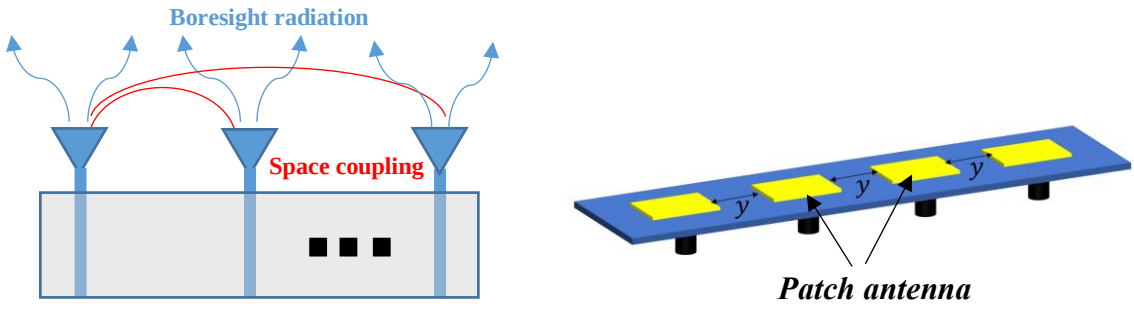

Figure. 3.1 Schematic of (a) spatial mutual coupling in an antenna array, (b) a tiled 1×4 patch antenna array.

Chapter I discusses different reported techniques [6-14] for counteracting mutual coupling in patch antennas mainly for a two antenna systems. In most of these techniques, modifications are to be incorporated post fabrication in the antenna design for achieving optimized performance, which impedes its implementation to a pre-existing array. For a tile-based array architecture, any alterations in the elemental design can disrupt the integration of the antenna with other connected electronics and may also alter the calibration settings. Hence, a need of a simple and easily integrable mutual coupling reduction technique which does not require any revamping of predesigned antenna array.

The present chapter proposes a metasurface superstrate (MS) based mutual coupling mitigation technique for an antenna array. The proposed approach is specifically tailored for operation between 8-8.5 GHz with 8.3 GHz as the reference frequency. This frequency band within the X-band is of strategic importance across multiple application domains including weather and surveillance radar systems, as well as military satellite communications (MILSATCOM). The proposed metasurface is to be designed as a single layer having low profile. Following which, it is tested for mutual coupling reduction in specially fabricated closely spaced 1×3 and 1×7 antenna arrays. The simulated and measured results are validated for reduction of mutual coupling. All the simulations are conducted in commercially available CST Microwave Studio software.

3.2. DECOUPLING MECHANISM IN METASURFACE DESIGN

In an array setting, the coupling of electromagnetic (EM) waves can occur from both the adjacent elements on either side of the antenna for a tiled configuration as obvious from Figure 3.1(b). The spatial mutual coupling, as represented in Figure 3.1(a), can be reduced if the spatial spreading of the EM waves generated by the antenna elements can be confined. The radiation from the antenna element can be illustrated using wave equation in frequency domain for a homogenous isotropic medium, given by,

$$\nabla^2 \boldsymbol{E} + k^2 \boldsymbol{E} = 0 \qquad (3.1)$$

where, $k = \omega\sqrt{\mu\varepsilon}$, is the wave number.

Laplacian of any vector field, $\nabla^2 \boldsymbol{V}$, determines the extend of spreading of the field in the space around a point and $\nabla^2 \boldsymbol{V} = 0$, corresponds to a steady state condition. Additionally, cross product of the vector is equal to zero i.e. $\nabla \times \boldsymbol{V} = 0$, indicates that the vector field is irrotational. Referring to Equation 3.1, $\nabla^2 \boldsymbol{E} \rightarrow 0$ will happen when the wave propagates in a medium with either $\mu \approx 0$ or $\varepsilon \approx 0$. Further, from Faraday's Maxwell equation, $\nabla \times \boldsymbol{E} = j\omega\mu \boldsymbol{H}$. If $\mu \approx 0$ then $\nabla \times \boldsymbol{E} \rightarrow 0$. Thus, if the radiation from the antenna can propagate through a mu-near-zero medium both the spatial spreading of electric field and the magnetic field interactions can be minimized, as known that $\boldsymbol{B} = \mu \boldsymbol{H}$, thus will result in reduction in leakage of the electromagnetic wave.

When an EM wave passes through a Negative Index Material (NIM), the direction of refraction is reversed compared to what would be predicted for a positive index material using Snell's law [15], as shown in Figure 3.2. Consequently, spatial spreading of the EM

waves from a radiating antenna can be minimized if it can propagate through a NIM, this confinement will prevent energy leakage to adjacent antenna elements and result in reduction of mutual coupling. Another interesting fact is that the phase velocity of the wave is directed opposite to the flow of energy (group velocity) in NIM. This behavior results in minimal phase variation along the propagation path. Since the phase variation is minimal, the wave's path is effectively unchanged, meaning that the electrical length remains constant. This property of the NIM results in no alteration in the resonant frequency of the antenna and thus no modifications required in the original antenna design. As mentioned in references [20-21], metamaterials designed with negative refractive index property when placed as a superstrate over patch antenna, can reportedly lead to gain enhancement by focusing the EM wave passing through the superstrate. The focusing nature and minimum phase variation property of negative index metamaterials are exploited to develop metasurface superstrate (MS) to minimize the spreading of the EM waves thus mitigating mutual coupling without reverting to modification in parent antenna design. Another advantage of metamaterial based focusing is the flat surface in contrast to the curved surfaces of traditional lenses, making it easy to mount and fabricate.

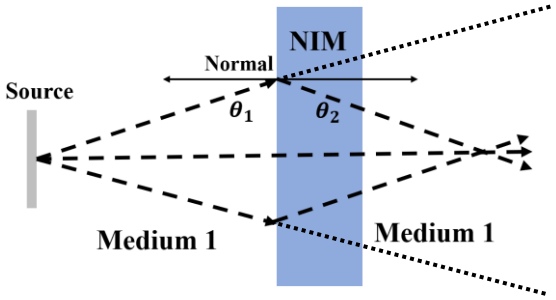

Figure 3.2. Schematic of negative refraction in NIM material

3.3. DESIGN AND SIMULATION

3.3.1. Metasurface unit cell

NIM MS unit cell with mu-near-zero property is realized by designing a planar split ring resonator (SRR) with two asymmetric I-shaped structures placed on the adjacent sides. Figure 3.3(a) shows the geometry of the unit cell. The SRR is printed on one side of a 0.8mm ($0.02\lambda o$ at 8.3GHz) thick Flame Retardant 4 (FR4) substrate. It may be mentioned here that the SRR structure is well known for creating magnetic response under EM

illumination [16]. In reference [17], I-shaped structures are placed horizontally for maximum current distribution leading to the electric response. Here, the SRR sandwiched between two horizontally placed I-shaped structures is used for designing the unit cell, thus giving an advantage of both magnetic and electric responses in a single cell. Periodic boundary conditions are applied on the four sides with the perfect electric conductor (PEC) in xz plane and perfect magnetic conductor (PMC) in xy plane. The simulation setup is shown in Figure 3.3(b).

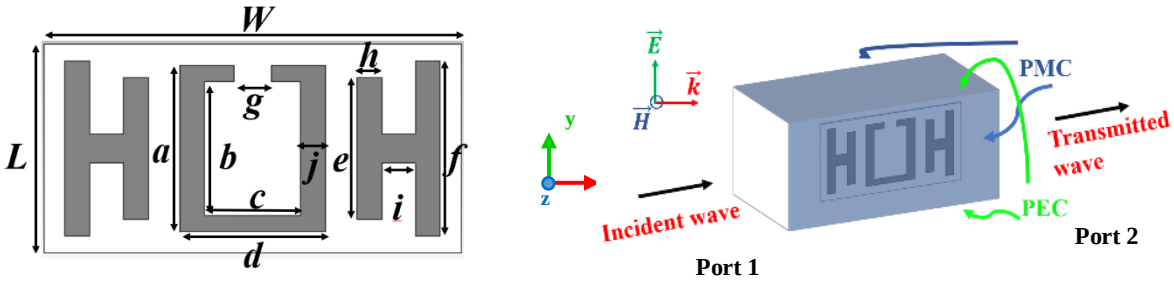

(a) (b)

Figure 3.3. (a) Layout of the proposed metasurface superstrate unit cell (b) Floquet port simulation setup of the unit cell.

The material properties are obtained by incorporating the scattering parameters in the algorithm described in reference [18]. The numerical simulation results show a strong rejection band in the frequency range of 8-8.6 GHz as drawn in Figure 3.4(a). A $\mu \approx 0$ region is observed from 7.6 – 9 GHz. The unit cell shows NIM region from 7 – 9 GHz, as seen from Figure 3.4(b). The optimized dimensions of the MS unit cell at 8.3 GHz is placed in Table 3.1. Field analysis is carried out at 8.3 GHz and presented in Figure 3.4(c) showing H-field propagation restriction along *x*-direction represented by low intensity blue arrows.

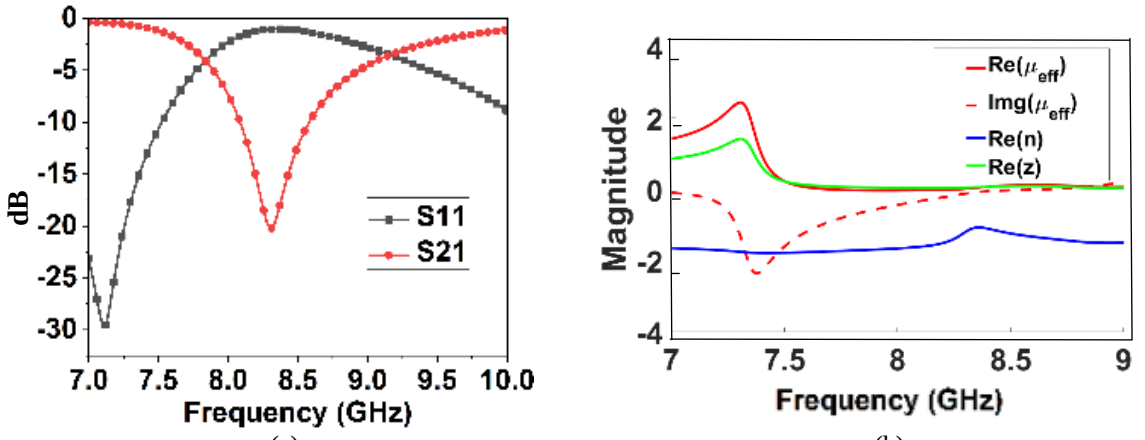

(a) (b)

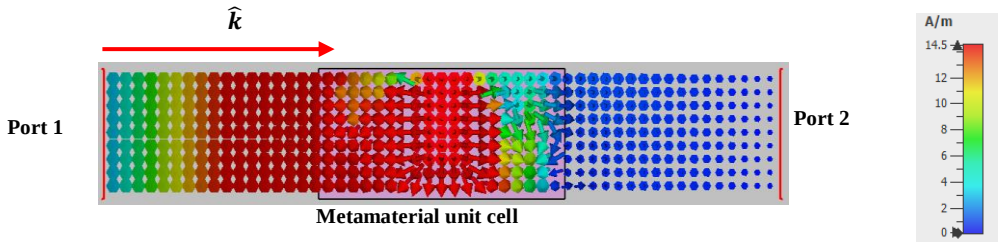

(c)

Figure 3.4. Simulated results of metasurface unit cell at 8.3 GHz (a) reflection and transmission coefficients, (b) real and imaginary part of permeability, μ_{eff}, real part of refractive index, η and real part of impedance, z ,(c) H-field distribution.

Parametric analysis

Parametric analysis is carried out to analyze the sensitivity of performance for different dimensions of the metamaterial unit cell. Figure 3.5 (a-c) shows the transmission characteristics with variation in dimensions of the unit cell. A rejection band is observed in the frequency range of 7-9 GHz with the variation of the gap width, g, from 0.7 to 1.0 mm with a step of 0.1 mm, refer Figure 3.5(a). Structural asymmetry in SRR is introduced by the gap, g, with respect to the electric-field plane of the incident wave, which gives rise to circulating current. The diminishing width of g induces a change in the peak intensity due to enhanced symmetry [19]. Stopband resonant frequency shifts towards higher frequency side with increase in the value of strip width, j, of the SRR, as depicted in Figure 3.5(b). Another parameter which shows marked change in transmission plots is the width, h, of the serifs of the I-shaped structure in vicinity to the SRR. Resonance frequency shifts from 8.5 to 8.0 GHz as h changes 0.2 mm to 0.8 mm with a step size of 0.2 mm, this is indicated in Figure 3.5(c).

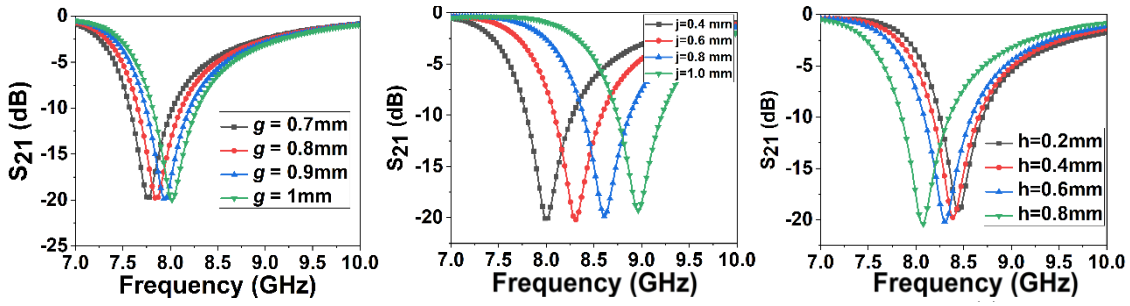

(b) (c)

Figure 3.5. Simulated S_{21} for the metasurface unit cell for different values of (a) gap width, g, (b) strip width , j, (c) serif-width, h.

Table 3.1 Optimized parameters of the metasurface unit cell at 8.3 GHz.

Parameter	***L***	***W***	***a***	***b***	***c***	***d***
Value (mm)	5	10	4	3.2	2.3	3.5
Parameter	***e***	***f***	***g***	***h***	***i***	***j***
Value (mm)	3.4	4.2	0.9	0.6	0.8	0.6

3.3.2. 1x3 antenna array

E-shaped patch antenna design, having same geometry as mentioned in **Chapter II,** is adopted here to get a wideband characteristic. A 1mm thick FR-4 substrate with dielectric constant, $\varepsilon_r = 4.3$ and loss tangent, $tan\delta = 0.025$, is employed for antenna fabrication. Single antenna element is designed to resonate at 8.3 GHz having bandwidth between 8-8.5 GHz, refer Figure 3.6. The optimized dimension of the antenna is summarized in Table 3.2. The return loss spectra shows that the designed antenna element has a -10dB bandwidth of 400 MHz (8.0-8.4 GHz), which is 4.87% in X-band, denoted by blue coloured plot in Figure 3.7(b).

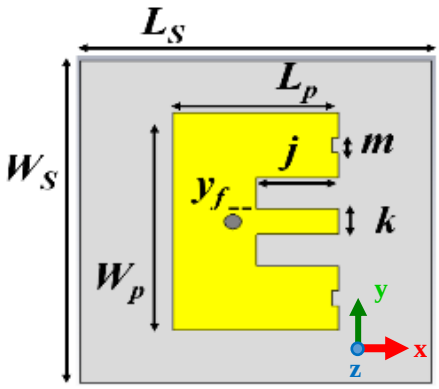

Table 3.2 Optimized parameters of single E-shaped antenna

Parameter	**Value (mm)**
Length of the ground plane (L_s)	16.80
Width of the ground plane (W_s)	17.50
Length of the patch (L_p)	7.90
Width of the patch (W_p)	11.80
Length of the slot (j)	3.90
Width of the slot (k)	1.70
Width of the slot (m)	0.80
Location of feed point in y - direction (y_f)	-1.1

Figure 3.6. Schematic representation of the single patch antenna dimensions

The single E-shaped antenna element discussed above is translated in *y*-direction to build a 1×3 linear array as shown in Figure 3.7(a). The edge-to-edge interelement spacing is kept same as $t = 0.16\lambda o = 5.7\ mm$ to get a closesly spaced array. Initially center element i.e. $Ant\ 2$, of the array is excited . A -10dB bandwidth of 4.38% and a mutual coupling (S_{12}) of -19 dB is observed and plotted in Figure 3.7(b). On comparing the antenna performance, as single element and in a 1×3 array environment, a reduction in the -10 dB bandwidth is observed, which can be attributed to coupling with other elements in vicinity.

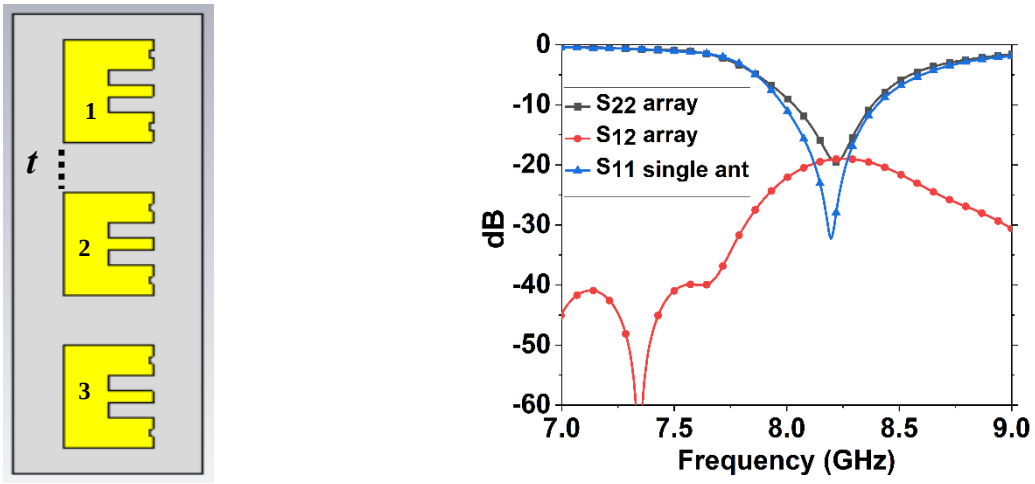

(a) (b)

Figure. 3.7. (a) Schematic diagram of the 1×3 antenna array. (b) *Simulated return loss,* S_{11} *of single antenna element (blue line) and* S_{22} *and* S_{12} *for* 1×3 *antenna array with only Ant* 2 *excited.*

3.3.3. 1×3 antenna array-metasurface assembly

The metasurface unit cell discussed in section 3.3.1 is replicated along *x* and *y* direction to form a 7×7 metasurface pane with a dimension of, $W_{MS} \times L_{MS} = 70\,mm \times 35\,mm$, as shown in Figure 3.8(a). The size of the metasurface sheet is ascertained to completely cover the 1×3 antenna array. The metasurface is placed as superstrate above the array, as illustrated in Figure 3.8(b), the height, z, is further optimized to effectively mitigate the coupling effects.

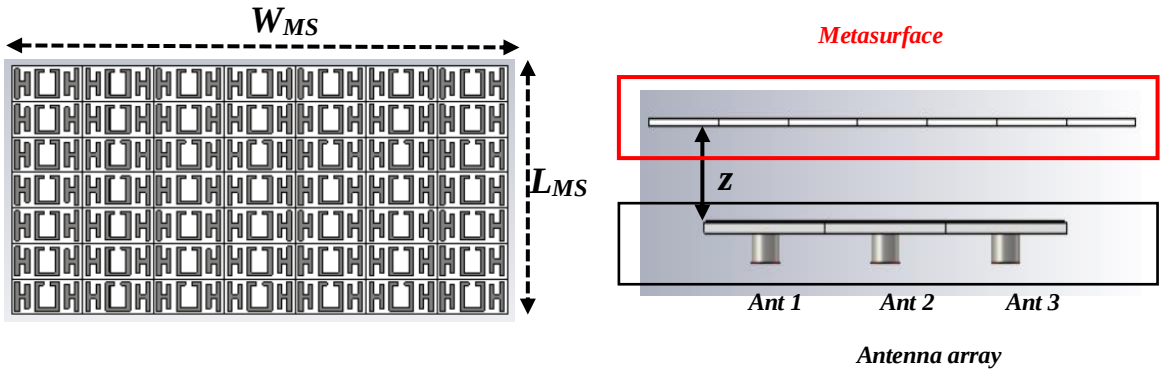

(a) (b)

Figure 3.8. (a) Simulated design of 7×7 metasurface array. (b) Schematic of placement of metasurface as superstrate above 1×3 antenna array.

Parametric studies

Simulations are performed to analyse the S_{22} and S_{12} for different values of placement height, z, varying from $7.5 - 10.5\ mm$ in steps of 1 mm. The metasurface parameters are taken from Table 3.1. The analysis of choosing the value of z is carried out by choosing best combination of reduced coupling and a good impedance matching. Superstrate placement height of $z = 9.5\ mm$ ($0.26\lambda o$ at 8.3 GHz) shows the optimal results as observed from Figures 3.9(a and b). A reduction of 13.9dB in mutual coupling is observed as compared to antenna without the MS. The effect of SRR gap and periodicity on the antenna-metasurface assembly for $z = 9.5\ mm$ is re-estimated by varying g and cell width, W. No significant effect on the mutual coupling values is observed within the operating -10 dB bandwidth of the antenna with g, as witnessed from the Figure 3.9(c). Increase in periodicity, however, lowers the coupling values as plotted in Figure 3.9(d).

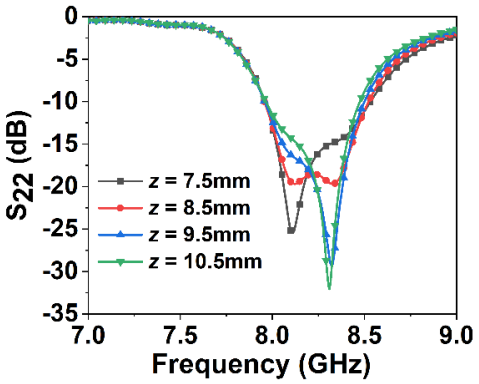

(a)

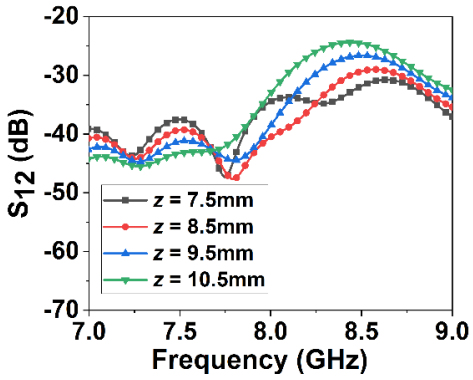

(b)

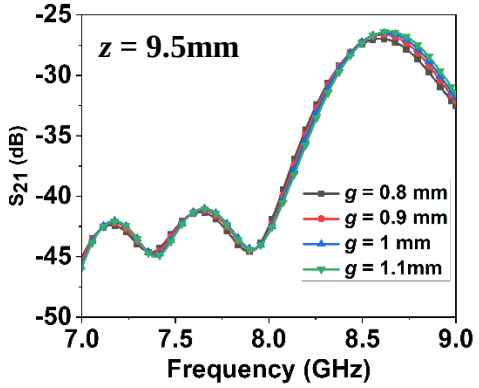

(c)

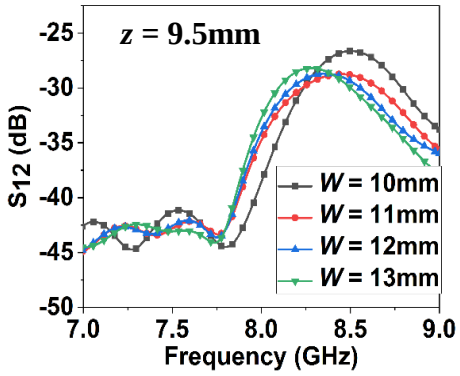

(d)

Figure 3.9. Parametric analysis: (a) S_{22} for different values of metasurface placement height, z and S_{21} for different values of (b) placement height, z, (c) gap width, g and (d) periodicity, W.

The metasurface designed with the optimized parameters is placed above the 1 × 3 antenna array and simulated reurn loss, S_{22} and mutual coupling, S_{12} , with only center antenna element, *Ant 2,* excited is plotted in Figure 3.10. The antenna array without (WO) MS shows a mutual coupling of -19.1 dB at 8.3 GHz. In presence of MS, the mutual coupling value is found to be -33.35 dB. A reduction of 14.25 dB in mutual coupling is observed for the array-metasurface assembly.

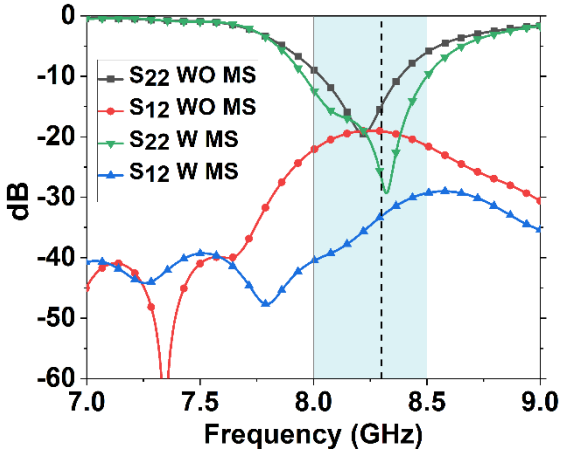

Figure 3.10. Simulated return loss S_{22} and mutual coupling S_{12} without (WO) and with (W) metasurface superstrate of 1 × 3 array.

A field distribution analysis is carried out at 8.3GHz to further verify the effect of the metasurface superstrate (MS) on the mutual coupling behavior of the 1 × 3 antenna array. Simulation is carried out by exciting *Ant 2* while both the neighboring elements, *Ant 1* and *Ant 3,* are terminated with a matched load. The magnetic field line distributions in *xoz*-plane WO the metasurface, spreads out with contours reaching adjacent elements. With placement of MS, the H-field distribution gets confined to the antenna surface, indicated by smaller and fewer contours near the superstrate as observed from Figures 3.11(a-b). Figures 3.11(c-d) shows the E-field distribution. The negative refractive index of the MS tends to focus the EM waves radiated by the antenna, evident from collimated beam in the direction of propagation above the MS, indicated by closed contour in Figure 3.11(d). For array WO metasurface, the surface current tends to spread and travel horizontally, interacting with the adjacent antenna elements as shown in Figures 3.11(e and f). In presence of metasurface, the coupling of magnetic field with the MS restricts surface

current interaction with the adjacent elements, as demonstrated by low intensity current density in Figure 3.10(f).

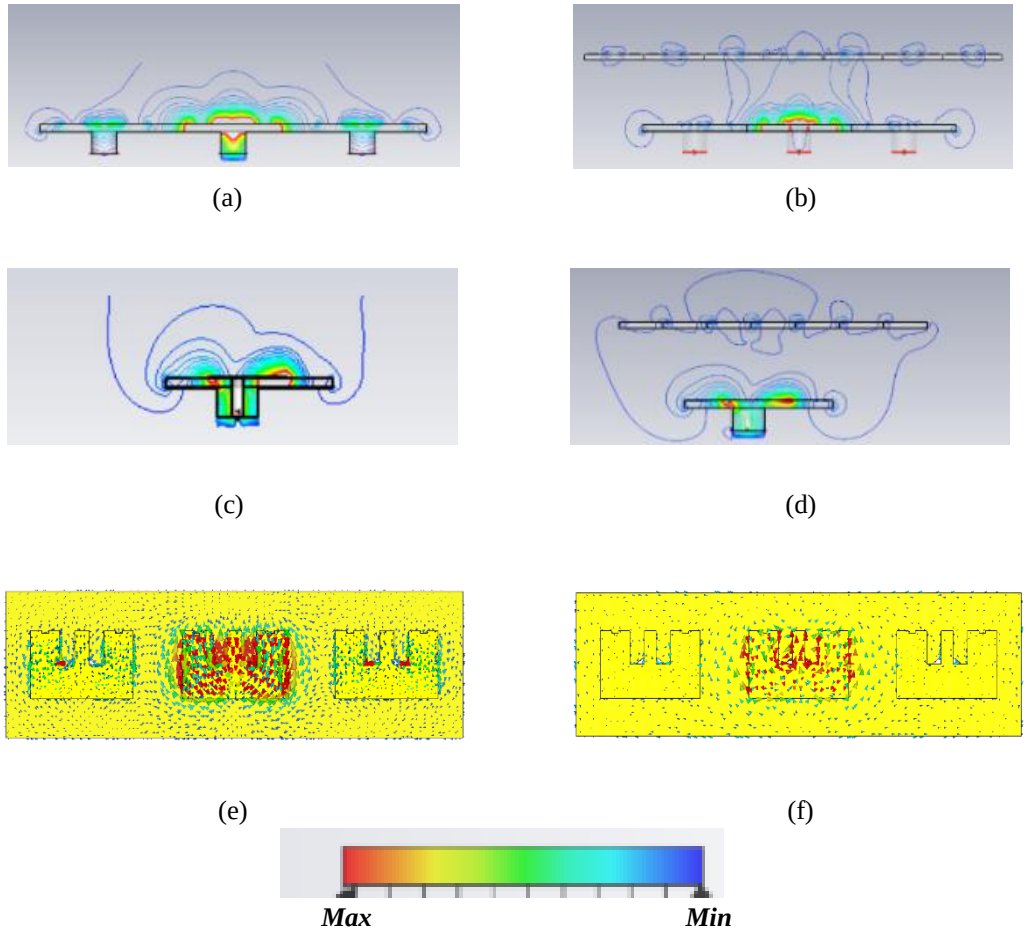

Figure. 3.11. Simulated field distribution at 8.3 GHz: H-field (a) WO metasurface, (b) with (W) metasurface; E-field (c) WO metasurface, (d) with(W) metasurface; and magnetic surface currents (e) WO metasurface, (f) W metasurface.

3.3.4. 1×7 array- metasurface assembly

The effectiveness of the proposed mutual coupling reduction technique is further validated, by extending it to a larger antenna configuration. The E-shaped patch element, employed in the design of the 1×3 antenna array discussed in Section 3.3.3, is utilized to design a 1×7 linear antenna array. Full coverage of the 1×7 array is ensured by using MS comprising of 7×12 metasurface unit cells . The superstrate is aligned and placed above the antenna array at an optimized height of $z = 10.5\ mm$ as shown in Figure 3.12(a). This positioning is chosen based on prior parametric studies to maximize coupling suppression without adversely affecting the primary radiation characteristics of the array. The mutual coupling performance is analyzed by exciting the central antenna element i.e., $Ant\ 4$, while keeping

the remaining elements terminated with matched loads. This method of excitation isolates the coupling behavior in a representative and symmetrical configuration. The simulated S-parameter results, illustrated in Figure 3.12(b), reveal an improvement in isolation. In particular, a mutual coupling level better than −23dB is achieved, with a reduction of 9.2 dB at the operational frequency 8.3 GHz as compared to the reference case without(WO) the MS. The final dimensions of the integrated structure, comprising of 1×7 antenna array and the MS, are $35\,mm \times 120\,mm \times 12.3\,mm$. These correspond to approximately $0.9\lambda_o \times 3.3\lambda_o \times 0.3\lambda_o$, where λ_o is the free-space wavelength at 8.3 GHz. This extended array serves as a practical testbed for evaluating the scalability and consistency of the proposed MS in mitigating mutual coupling across multiple elements.

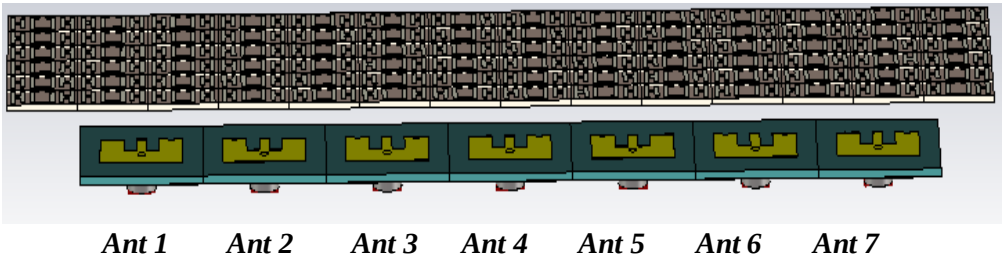

(a)

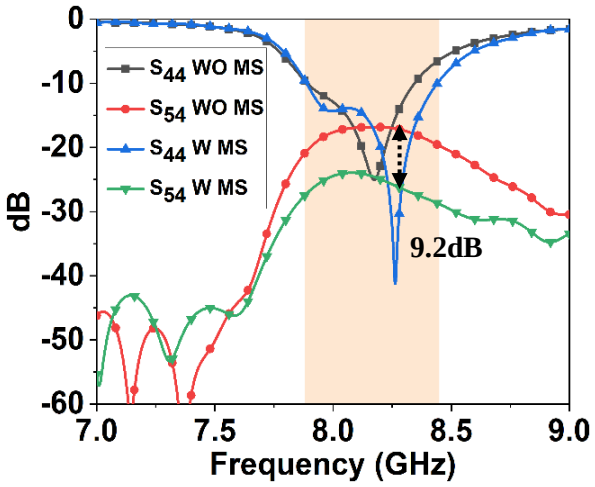

(b)

Figure 3.12. (a) Schematic of metasurface superstrate over 1×7 antenna array, (b) simulated S_{44} and S_{54} of the 1×7 array WO /W metasurface superstrate with only Ant 4 excited.

3.4. IMPLEMENTATION AND PERFORMANCE EVALUATION

3.4.1. S_{11} and radiation pattern measurement technique

S_{11} measurement

The S_{11} measurements of the antennas in this study were performed using an Agilent E8362C PNA-series Vector Network Analyzer (VNA). Prior to the measurements, a thorough calibration is conducted using the Agilent 85052D calibration kit, employing the short, open, and broadband load standards as shown in Figure 3.13.

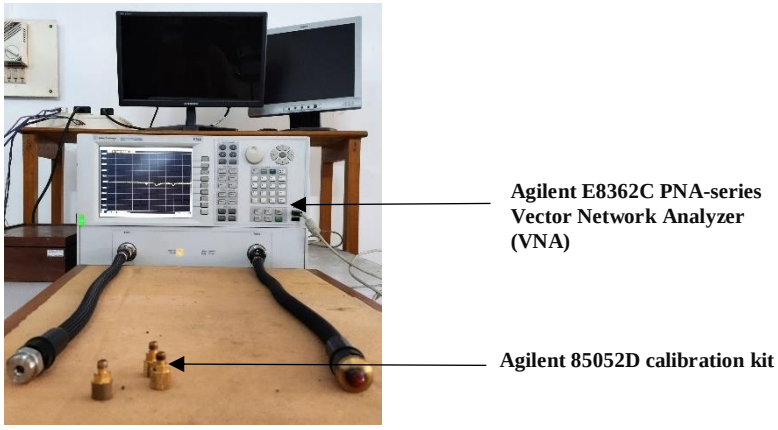

Figure 3.13 Agilent E8362C PNA series VNA and Agilent 85052 calibration kit.

Radiation pattern measurement

The radiation pattern measurements is conducted using an automated antenna measurement system from Diamond Engineering, USA (Model: DAMS 6000 Series) as shown in Figure 3.14. The setup includes a precision turntable equipped with an attachable mount, enabling full spherical measurements with a load capacity of 2.3 kg. The system provides a high angular resolution of 0.06° in both azimuth and elevation planes.

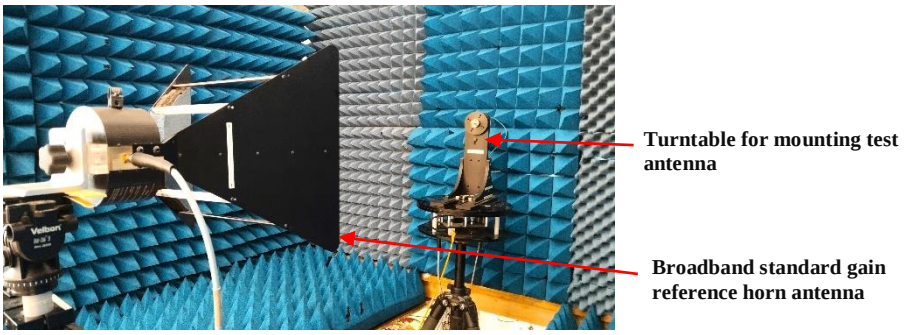

Figure 3.14 Automated antenna measurement system from Diamond Engineering.

3.4.2. Fabrication and performance study of 1×3 antenna array-metasurface assembly

The MS and antenna arrays are fabricated on FR4 substrate with dimensions mentioned in Tables 3.1 and 3.2 respectively, using chemical etching technique. Figures 3.15(a-b) shows 1×3 fabricated antenna array and corresponding 7×7 panel of metasurface. All the three antennas are coaxially fed using SMA connectors. The return loss and mutual coupling is measured using Agilent E8362C Vector Network Analyzer (VNA) with only *Ant 2* excited. The MS is placed above the antenna array using 3-D printed PLA stubs of height, z = 9.5 mm. The overall dimension of the array-MS assembly is $70\,mm \times 35\,mm \times 11.3\,mm$ which is $1.9\lambda_o \times 0.9\lambda_o \times 0.30\lambda_o$, at 8.3GHz. Figures 3.15(c-d) show the front and the lateral view of the assembled 1×3 array with the superstrate, respectively. Figures 3.16(a-b) show the measured and simulated return loss, S_{22} and mutual coupling, S_{12} and S_{32} parameters of the 1×3 array without (WO) and with (W) the MS. The observed discrepancies between the measured and simulated results can be primarily attributed to fabrication tolerances and some variations in the height of the 3D-printed support structure used to position the metasurface superstrate (MS). With the MS in place, the mutual coupling reduces to below −25 dB across the operational frequency band, with isolation values ranging from -31.2 dB to −38.2 dB. The maximum observed reduction in coupling reaches up to 14.37 dB compared to the configuration without the MS. In addition to enhanced isolation, the impedance bandwidth of the antenna also shows a notable improvement. The measured −10 dB bandwidth increases from 3.11% to 5.12%, corresponding to a frequency range of 8.17 GHz to 8.61 GHz. Similar enhancements in bandwidth have been reported in earlier studies, such as [14] and [20], and are in corroborated with the simulation results.

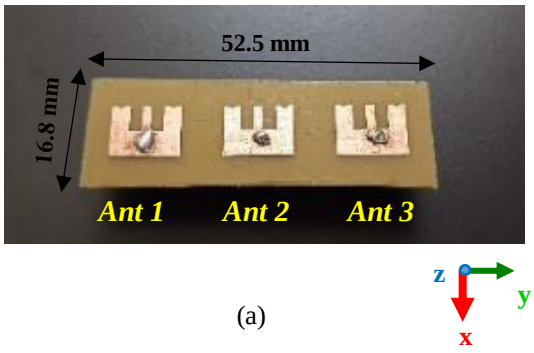

(a)

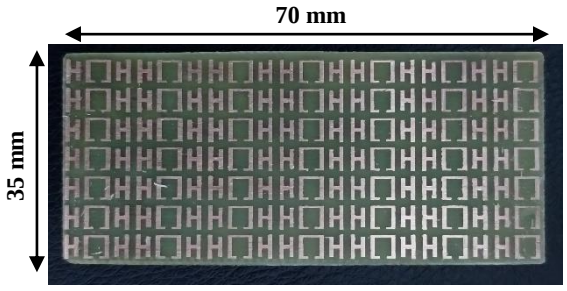

(b)

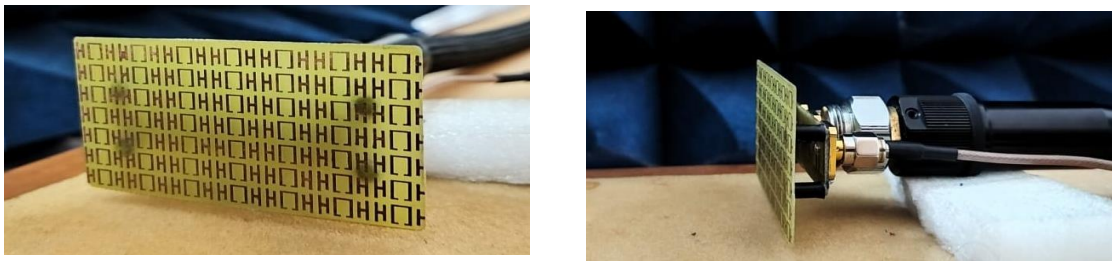

(c) (d)

Figure 3.15. Fabricated (a) 1×3 antenna array (b) metasurface with 7×7 unit cells. 1×3 array-MS assembly (c) front view and (d) lateral view.

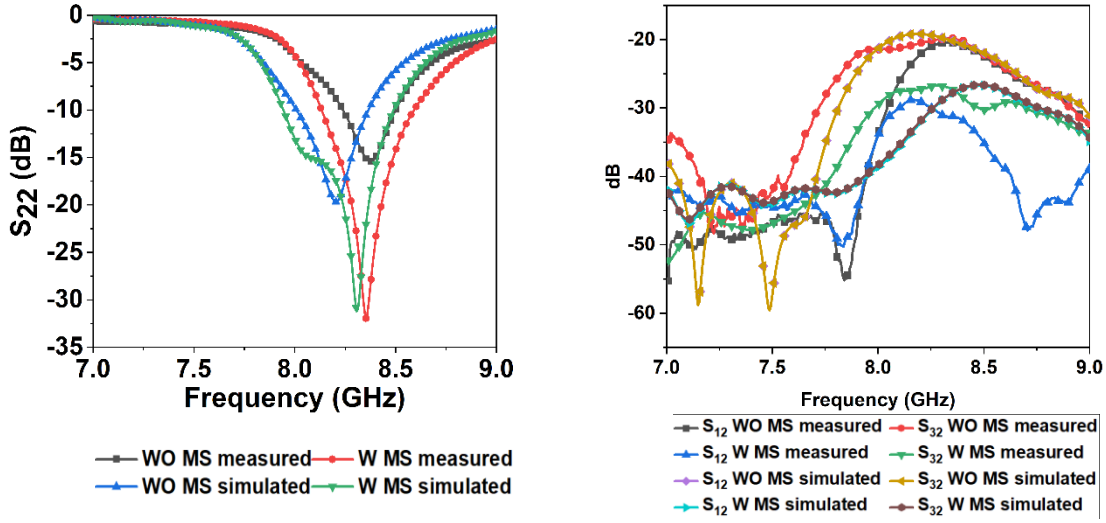

(a) (b)

Figure 3.16. Measured and simulated (a) S_{11} and (b) S_{21} and S_{31} parameters of the array WO/W metasurface superstrate.

2-D far-field active radiation pattern is measured for 1×3 antenna array with *Ant 2* excited and $Ant\ 1$ and $Ant\ 3$ terminated with a 50Ω X-band match load using DAMS Antenna Measurement system as shown in Figure 3.14. The measured active radiation pattern in H-plane (*xoz*-plane) and E-plane (*yoz*-plane) at 8.3 GHz WO/W superstrate is shown in Figures 3.17(a-b). There is an improvement in cross polarization levels in the active radiation pattern. The improvement in cross-polarization levels are due to reduction in mutual coupling between the adjacent elements, similar observations are reported in [30]. Respective, measured gain levels of the center element i.e. *Ant 2* excited is shown in Figure 3.18. From Figure 3.18, it is evident that there is an increase in the gain levels of the antenna with MS. The improvement in gain could be due to two reasons, firstly the negative

refractive index of the metamaterial superstrate helps in collimating the E-field in broadside direction as also observed in field analysis, refer to Figure 3.11(d). The second possible reason could be similar to the phenomenon reported in [21], where cavity type effect takes place between of the superstrate and the array when positioned at an optimal height. The mu-near-zero, $\mu \approx 0$ property of the metasurface helps in confining the magnetic field, which minimizes energy leakage to adjacent elements and thus reduces the mutual coupling and enhances the gain of the antenna. The center element with MS shows an enhanced -10 dB bandwidth of 5.12% in X-band. The isolation is improved to 31.02 dB at 8.3GHz. The radiation pattern shows enhanced cross polarization levels to below 30 dB in both H- and E-planes. Table 3.3 consolidates the performance of the array-MS system at 8.3GHz.

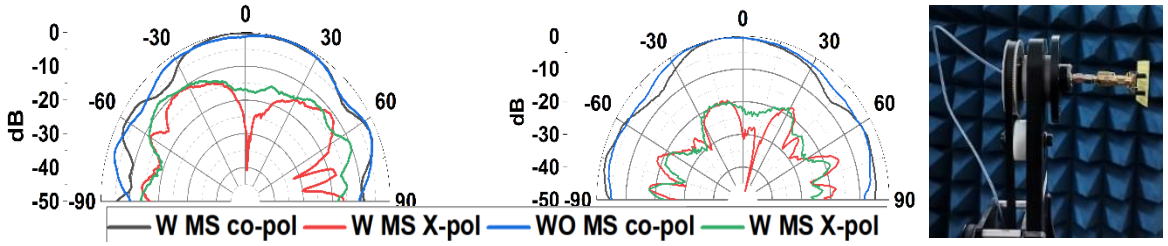

(a) (b)

Figure 3.17. Measured active radiation pattern in (a) *H*-plane and (b) E-plane.

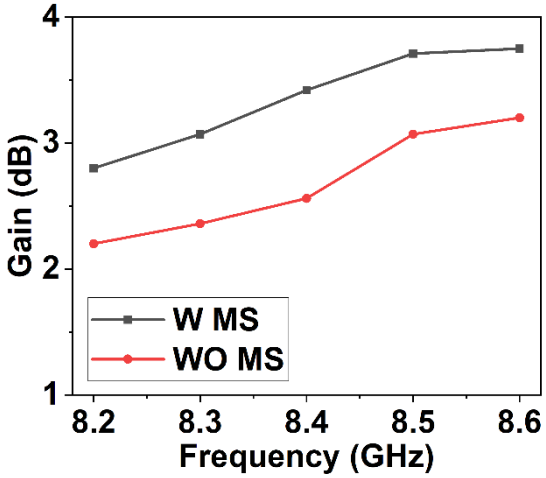

Figure 3.18. Measured gain of the 1×3 array with center element excited WO and W metasurface superstrate.

Table 3.3 Performance of 1 × 3 antenna array with only center element excited at 8.3GHz

Center element excitation mode	**Bandwidth (%)**	**Mutual coupling (dB)**	**Gain (dB)**	**Cross polarization (dB)**	
				H –plane	**E -plane**
Without(WO) MS	3.11	-20.47	2.36	16.61	23
With (W) MS	5.12	-31.02	3.2	34.46	31

The performance of the 1×3 antenna array is further investigated under practical excitation conditions i.e. when all the antenna elements are simultaneously energized using a 4-way power divider. The configuration of this simultaneous excitation setup is depicted in Figure 3.19(a). In this arrangement, three output ports of the power divider are connected to the individual antenna elements of the array, while the fourth port is terminated with a matched 50Ω load to prevent signal reflections and ensure equal power distribution. The reflection characteristics at input port of the power divider, with the array is measured for both without (WO) and with (W) the MS. The return loss plots are presented in Figure 3.19(b). Additionally, the far-field radiation patterns corresponding to these two configurations are illustrated in Figures 3.20(a–b).

The return loss results shown in Figure 3.19(b), shows the incorporation of the MS leads to an improvement in the S_{11} parameter. This indicates enhanced impedance matching of the array under simultaneous excitation. Notably, the resonance frequency remains unchanged upon placement of the superstrate, demonstrating that the MS structure does not perturb the fundamental resonant behavior of the array.

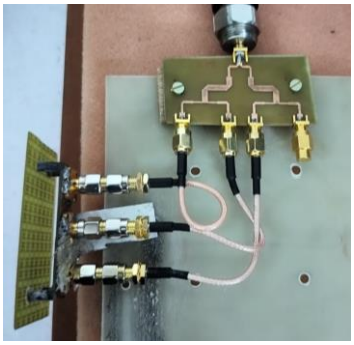

(a)

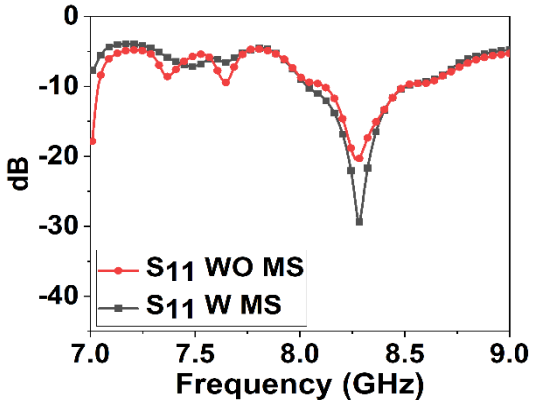

(b)

Figure 3.19. (a) Arrangement of 1×3 array for simultaneous excitation of all the elements using 4-way power divider (b) S_{11} of the array WO and W metasurface superstrate.

These results confirm that the proposed metasurface superstrate not only aids in mutual coupling suppression but also maintains the intrinsic impedance characteristics and bandwidth performance of the antenna array during simultaneous operation of all the elements.

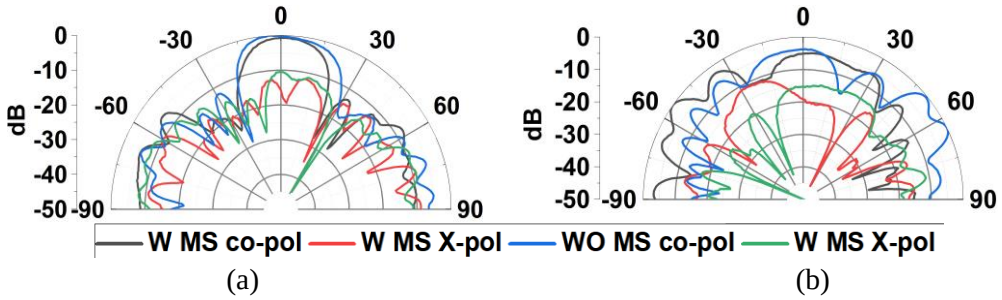

Figure 3.20. Measured radiation pattern with simultaneous excitation of all the elements for 1 × 3 array in (a) H-plane and (b) E-plane.

3.4.3. Fabrication and performance study of 1×7 antenna array-metasurface assembly

The effect of the metasurface superstrate for a larger antenna array is evaluated. Here coaxially-fed 1 × 7 antenna array is fabricated as shown in Figure 3.21(a). MS with 7 × 12 unit cells configuration is developed, as mentioned in Section 3.3.4, and positioned at a vertical distance of $z = 10.5\ mm$ above the antenna array using low-permittivity foam spacers to ensure minimal electromagnetic interference and structural support. The physical placement and alignment of the MS over the antenna array are illustrated in Figure 3.21(b).

The performance evaluation is carried out by exciting only the central element of the array i.e., *Ant 4*, while all the other ports are terminated with matched loads. Figure 3.21(c) presents the measured return loss, S_{44} and mutual coupling S_{54} under this excitation condition. In terms of impedance characteristics, the array exhibits an improved −10 dB bandwidth of 4.48%, spanning from 8.28 to 8.66 GHz. The mutual coupling is reduced by 9.24 dB at the resonance frequency of 8.3 GHz, with a maximum measured isolation reaching up to 34.03 dB as depicted by the S_{54} curve. Importantly, the operational bandwidth improves with the inclusion of the MS, demonstrating the non-intrusive nature of the proposed approach.

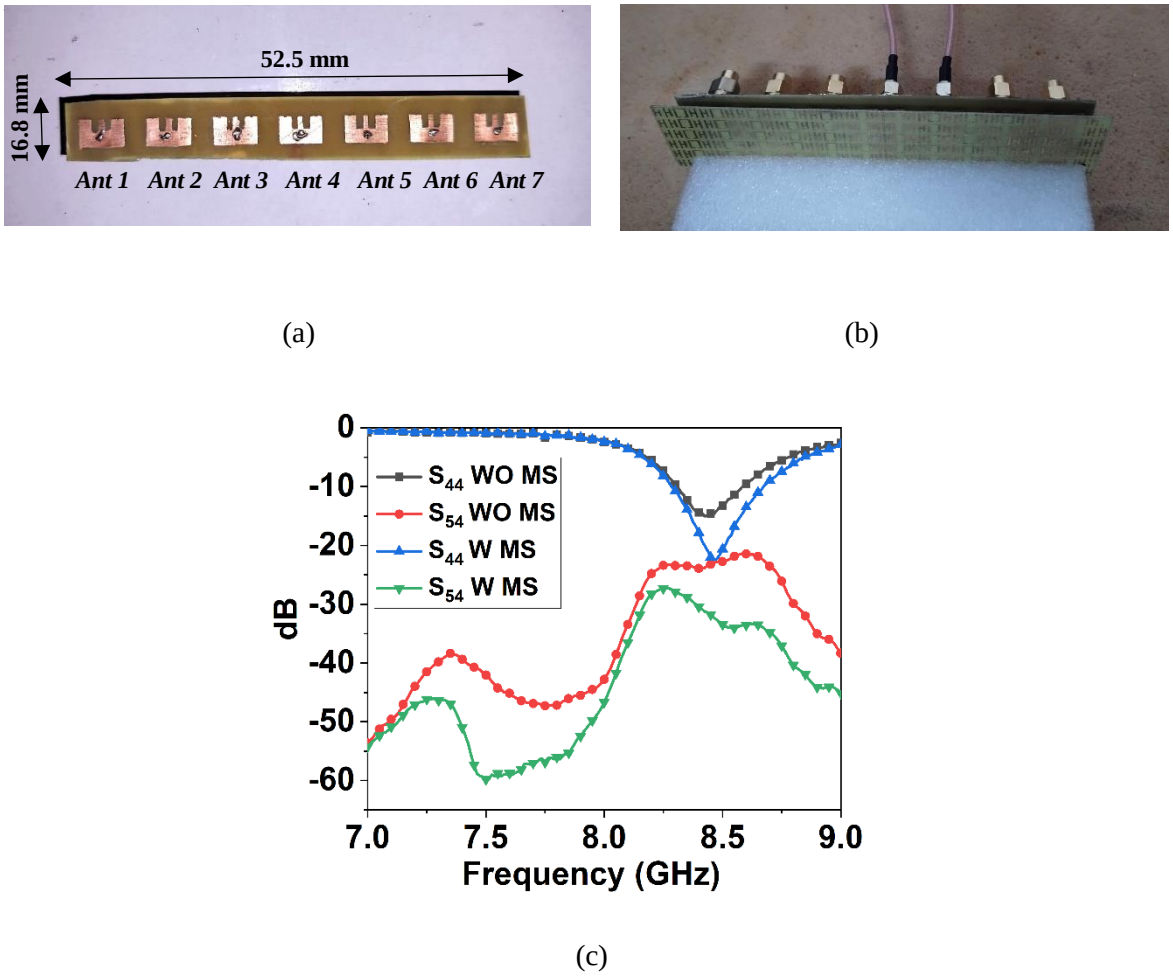

Figure 3.21. (a) Photo graph of fabricated 1 × 7 coaxially fed antenna array (b) set-up with metasurface superstrate placed. (c) Return loss and mutual coupling of 1 × 7 antenna array WO/W metasurface superstrate with only Ant 4 excited.

3.5. CHAPTER SUMMARY

This chapter proposes and experimentally validates an effective approach for mutual coupling reduction in linear patch antenna array configurations. A metasurface (MS) superstrate-based technique is introduced to significantly suppress mutual coupling in both 1×3 and 1×7 antenna arrays. The designed MS is single-layered and low-profile, resulting in an overall thickness of only 11.3 mm for the 1×3 antenna-MS assembly and 12.3 mm for the 1×7 antenna-MS assembly. Measurements confirm that mutual coupling below –25 dB is achieved across a 5.12% bandwidth in the X-band, with a maximum reduction of 14.37 dB observed in the 1×3 array. The active radiation pattern of the 1×3 array further demonstrates improved cross-polarization performance, with levels of –34.46 dB in the H-plane and –31 dB in the E-plane, without introducing significant distortion in the radiation

characteristics. One of the key advantages of the technique is that the array performance remains consistent, and the resonant frequency is unaffected even when all elements are excited simultaneously. Validation in the 1×7 antenna array confirms the effectiveness of the approach, where mutual coupling reduction is maintained across the entire operational bandwidth, with a notable reduction of 9.2 dB at 8.3 GHz. The proposed technique requires no modification to the original antenna element design after theplacement of the metasurface superstrate. Additionally, the use of the MS improves cross-polarization performance and broadens the operational bandwidth, while maintaining compact physical dimensions. These advantages, combined with enhanced electromagnetic isolation, highlight the practical viability of the proposed technique for large-scale antenna array applications.

References

[1]. T. C. Cheston and J. Frank. Phased array radar antennas. In *Radar Handbook*, M. I. Skolnik, Ed. New York: McGraw-Hill, 1990, chapt. 7.

[2]. Wei, X., Wang, G., Wang, Y., Zou, X., Tian, C., Bai, H., Yu, Z., & Cai, T. Metasurface-based bandwidth and isolation enhancement for compact H-plane coupled antennas. *Journal of Physics D: Applied Physics*, 57(13):135002, 2023. DOI:10.1088/1361-6463/ad13c7

[3]. Emadeddin, A., Shad, S., Rahimian, Z., & Hassani, H. High mutual coupling reduction between microstrip patch antennas using novel structure. *AEU - International Journal of Electronics and Communications*, 71:152–156, 2016. DOI:10.1016/j.aeue.2016.10.017

[4]. Singh, Hema, et al. Mutual Coupling in Phased Arrays: A Review. *International Journal of Antennas and Propagation*, 2013:1–23, Jan. 2013. DOI:10.1155/2013/348123

[5]. Volmer, C., Weber, J., Stephan, R., Hein, M.A. A descriptive model for analyzing the diversity performance of compact antenna arrays. *IEEE Transactions on Antennas and Propagation*, 2009. DOI:10.1109/TAP.2008.2011244

[6]. Tunio, Irfan Ali, et al. Mutual coupling reduction in patch antenna array using combination of shorting pins and metallic walls. *Progress in Electromagnetics Research C*, 107:157–171, Jan. 2021. DOI:10.2528/pierc20082803

[7]. Ou, Yangsong, et al. Two-element compact antennas decoupled with a simple neutralization line. *Progress in Electromagnetics Research Letters*, 65:63–68, Jan. 2017. DOI:10.2528/pierl16111801

[8]. Zhang, S., and G. F. Pedersen. Mutual coupling reduction for UWB MIMO antennas with a wideband neutralization line. *IEEE Antennas and Wireless Propagation Letters*, 15:166–169, 2015.

[9]. Naser-Moghadasi, Mohammad, et al. Compact EBG structures for reduction of mutual coupling in patch antenna MIMO arrays. *Progress in Electromagnetics Research C*, 53:145–154, Jan. 2014. DOI:10.2528/pierc14081603

[10]. K. Wei, J. Y. Li, L. Wang, Z. J. Xing, R. Xu. Mutual coupling reduction by novel fractal defected ground structure band-gap filter. *IEEE Transactions on Antennas and Propagation*, 64(10):4328–4335, 2016.

[11]. Wang, Z., Zhao, L., Cai, Y., Zheng, S., & Yin, Y. A meta-surface antenna array decoupling (MAAD) method for mutual coupling reduction in a MIMO antenna system. *Scientific Reports*, 8(1), 2018. DOI:10.1038/s41598-018-21619-z

[12]. F. Liu, J. Guo, L. Zhao, G.-L. Huang, Y. Li and Y. Yin. Dual-band metasurface-based decoupling method for two closely packed dual-band antennas. *IEEE Transactions on Antennas and Propagation*, 68(1):552–557, Jan. 2020. DOI:10.1109/TAP.2019.2940316

[13]. Li, M., Mei, J., Yang, X., Zeng, D., & Yi, Z. Isolation enhancement based on metasurface for dual-band E/H-plane coupled antenna array. *IEEE Antennas and Wireless Propagation Letters*, 1–5, 2024. DOI:10.1109/lawp.2024.3386677

[14]. Mark, R., Rajak, N., Mandal, K., & Das, S. Metamaterial based superstrate towards the isolation and gain enhancement of MIMO antenna for WLAN application. *AEU - International Journal of Electronics and Communications*, 100:144–152, 2019. DOI:10.1016/j.aeue.2019.01.011

[15]. J. B. Pendry. Negative refraction makes a perfect lens. *Physical Review Letters*, 85(18):3966–3969, Oct. 2000.

[16]. Zhou, J., Koschny, T., & Soukoulis, C. M. Magnetic and electric excitations in split ring resonators. *Optics Express*, 15(26):17881, 2007. DOI:10.1364/oe.15.017881

[17]. Jain, Prince, et al. I-shaped metamaterial antenna for X-band applications. *Proceedings of 2017 Progress in Electromagnetics Research Symposium - Spring (PIERS)*, May 2017. DOI:10.1109/piers.2017.8262229

[18]. A. Jafargholi and J. H. Choi. Mutual coupling reduction in an array of patch antennas using CLL metamaterial superstrate for MIMO applications. *IEEE Transactions on Antennas and Propagation*, 67(1):179–189, Jan. 2019. DOI:10.1109/TAP.2018.2874747

[19]. Kitayama, D., Pander, A., & Takahashi, H. Analysis of asymmetry in active split-ring resonators to design circulating-current eigenmode: demonstration of beamsteering and focal-length control toward reconfigurable intelligent surface. *Sensors*, 22(2):681, 2022. DOI:10.3390/s22020681

[20]. Alibakhshikenari, M., Virdee, B. S., Benetatos, H., et al. An innovative antenna array with high inter-element isolation for sub-6 GHz 5G MIMO communication systems. *Scientific Reports*, 12:7907, 2022. DOI:10.1038/s41598-022-12119-2

[21]. S. Benny, S. Sahoo, and A. Mukundan. Study on impact of mutual coupling on performance of dual polarized phased array antenna. *Advances in Electromagnetics*, 11(2):15–22, May 2022.